An LED-only BRDF Measurement Device

Moshe Ben-Ezra, Jiaping Wang and Bennett Wilburn
Microsoft Research Asia

{mosheb,jiapw,bwilburn}@microsoft.com

Xiaoyang Li and Le Ma*
Tsinghua University

xl99@cornell.edu

l-ma03@mails.tsinghua.edu.cn

Abstract

Light Emitting Diodes (LEDs) can be used as light detectors and as light emitters. In this paper, we present a novel BRDF measurement device consisting exclusively of LEDs. Our design can acquire BRDFs over a full hemisphere, or even a full sphere (for the bidirectional transmittance distribution function BTDF), and can also measure a (partial) multi-spectral BRDF. Because we use no cameras, projectors, or even mirrors, our design does not suffer from occlusion problems. It is fast, significantly simpler, and more compact than existing BRDF measurement designs.

1. Introduction

Measuring and predicting (rendering) the appearance of objects under different illumination and viewing conditions is critical for many applications in computer graphics and computer vision. An important component of appearance information is the Bidirectional Reflectance Distribution Function, or BRDF. The BRDF is defined as the ratio of reflected radiance exiting from a surface in a particular direction $\Omega_e = (\theta_e, \phi_e)$, to the irradiance incident on the surface from direction $\Omega_i = (\theta_i, \phi_i)$, for a particular wavelength λ [13].

$$f_r(\Omega_i, \Omega_e, \lambda) = \frac{dL(\Omega_e, \lambda)}{dE(\Omega_i, \lambda)} \qquad (1)$$

Due to its high dimensionality, measuring a BRDF is a complex and time consuming process. Traditionally, BRDFs were measured using gonioreflectometers, expensive special-purpose devices that mechanically move the light source and the detector from one position to another. Taking advantage of the reciprocity of the BRDF accelerated this process[18], but it remained very expensive and time consuming.

In 1992, Ward showed that an anisotropic BRDF could be captured much more efficiently by using a curved mirror to capture multiple reflected rays in parallel[21]. Curved mirrors were later used in several other BRDF measurement devices [2, 19, 9, 8, 5]. Marschner *et al.* [10] and Matusik at al.[11] efficiently captured isotropic BRDFs by using curved

material samples (usually cylinders or spheres) and capturing multiple orientations at once. Projector-camera systems can significantly decrease the BRDF measurement time because they make many measurements in parallel without any moving parts. Example methods include kaleidoscopic mirror arrangements [7], curved mirror arrangements [19] and light stages [14]. Recently, Ghosh *et al.* proposed an efficient way to capture low-order parametric BRDFs using illumination basis functions [5] that optically low-pass the measurement (thus avoiding aliasing).

Despite much work in this area, BRDF capture, and in particular fast acquisition of high-resolution BRDFs, remains quite challenging. Most of the methods mentioned above require a large, sophisticated setup with a camera and mirrors, and some also suffer from occlusions. Some methods require specially shaped material samples, while others require that the samples be placed inside the device. Such systems cannot be used easily outside the lab for data acquisition in the field. Moreover, because the dynamic range of BRDFs is typically quite large, projector-camera systems must take multiple exposures in order to capture high dynamic range measurements. This limits their maximum measurement rates. As an example, the system of Ghosh *et al.* [5], which captures roughly two HDR measurements a second, is considered very fast.

In this paper, we use the dual functionality of LEDs as light emitters and photodetectors to construct a BRDF measurement device. Because our device has no mirrors, projectors, cameras, or moving parts, it is simpler, smaller and faster than existing designs.

1.1. Contributions

We investigate the suitability of LEDs as analog light detectors by measuring of their response functions, dynamic ranges, response times and modulations. We present the methods and the results of our measurements.

We also present a design for a BRDF measurement device consisting exclusively of LEDs. The advantages of our design include: (i) Our design has no moving parts, no camera, no projector, nor even mirrors; as a result our design can be made very compact and easily portable. (ii) Our design does not suffer from occlusions, and it can measure over a compete hemisphere, or even a complete sphere (for BTDF
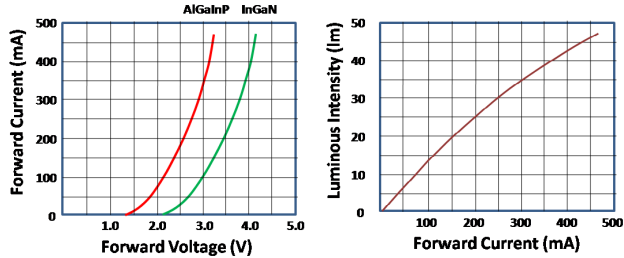
Figure 1. **Current and function of voltage, and intensity as function of current for the LEDs used in this paper. While current is non-linear with resect to voltage, intensity is nearly linear with current** (source: manufacturer's data).

measurement). We are not limited by an isotropy assumption. (iii) LEDs have very fast response times and high dynamic range, very desirable qualities for BRDF measurement. Our design can also use multiplexed illumination to increase SNR and speed. (iv) LEDs emit light and are sensitive to specific bandwidths allowing (partial) multi-spectral BRDF measurement.

The limitations of our method are: (i) Like all non confocal BRDF measuring methods, our method cannot measure the exact retro-reflected rays since an LED cannot simultaneously emit and detect light. (ii) The achievable resolution using discrete LEDs device, though relatively high, is still lower than possible with VLSI devices such as projector-camera setups. This limitation is relaxed by the ability to acquire BRDF using multiplexed illumination and illumination basis functions.

2. The LED as an Emitter and a Detector

The first reference to a light emitting diode (LED) was by Henry J. Round in 1907[15]. He touched a metal wire to a silicon carbon (SiC) crystal and noticed that the material gave off light when he passed a current through it (a phenomenon called *electroluminescence*). SiC-based *P-N* junction LEDs appeared in the late 1960s. These were blue LEDs emitting light at 470nm. These SiC based LEDs , however, were very inefficient; the best ones had an efficiency of only 0.03% [4]. Extensive research and development from the 1960's through the 1990's[1] lead to the development of much brighter LEDs. More about the history of LEDs can be found in [17]. Today, there are many different types of LEDs made from many different materials (GaAs, GaN, GaP, GaAsP). In this paper we use only two varieties of LEDs: aluminium gallium indium phosphide (AlGaInP, used for red, orange and yellow LEDs) and indium gallium nitride (InGaN, used for blue, green and turqoise LEDs). White LEDs are actually InGaN LEDs with a phosphor to convert the blue light to white.

---

[1] At IBM, GE, Lincoln Laboratories, MIT, HP, TI, Philips, AT&T, Bell Laboratories, RCA and Japanese Nichia Chemical Industries, to name a few locations.
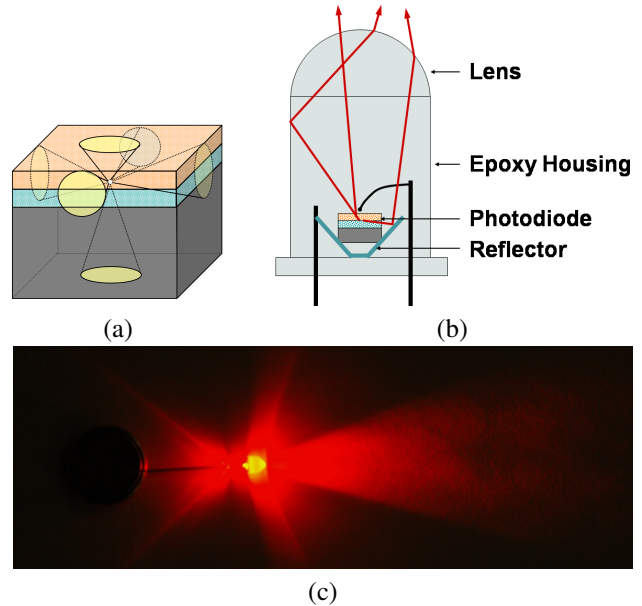

(a) (b)

(c)

Figure 2. **Optical properties of LEDs: (a) due to total internal reflection, light can escape from a cubical photodiodes in six escape cones. (b) the light from the escape cones is reflected from a tiny reflector inside the LED and then shaped into a beam with predefined angle by the transparent epoxy encapsulation that forms a light duct (using total internal reflection) and a lens. (c) Light redirection is not perfect and some 'stray light' escapes through the back and sides of the LED.**

2.1. Electroluminescence Properties of LEDs

When enough voltage is applied to an LED, current flows through the active region of the device. In an ideal LED, every electron injected into the active region would cause a photon to be emitted. Assuming constant temperature, the relationship between the emitted light and the current is nearly linear over a small range of current values. Current-voltage and current-intensity relationships are usually given by the LED manufacturer. Fig. 1 shows typical curves for the AlGaInP and InGaN LEDs used in our device. We see that the current is not linear with respect to voltage, but the intensity does increase nearly linearly with current, especially at low currents. We exploit this linearity for our calibration process.

Photodiodes can also be used as photodetectors, although LEDs are not optimized for this purpose. Dietz *et al.*, for example, used LEDs as binary transceivers to construct a low cost digital communication device[3]. The spectral response of LEDs depends on the wavelength they emit. In general, LEDs are sensitive to light of their own wavelength or shorter. Thus, a red LED will respond to light emitted from a blue led, but not vice versa. Mims *et al.* used this characteristic to construct a low cost sunlight photometer [12]. Because LEDs are not intended to be used as photodetectors, manufacturers do not provide specifications about their response function, spectral sensitivity, or dynamic range. This

information is critical for our design, so we must measure it ourselves. In section 4, we describe how we do this.

2.2. Optical Properties of LEDs

The physics of light emission from LEDs is such that it can escape the die only at certain specific angles called *escape cones*. Fig 2(a) shows an example for a rectangular die, which has one escape cone on each face. A small reflector and an epoxy housing, such as the popular T1 housing shown in Fig 2(b), shapes the light beam toward the desired viewing direction and angles. The viewing cone of the T1 LED is clearly visible in Fig 2(c). The critical observation for our design is that some light escapes the LED though the sides and back of the LED. We must ensure that stray light from one emitting LED does not interfere with neighboring sensing LEDs.

3. BRDF Capture Device Basic Design

Fig 3 describe the structure and basic operation of our design. Similar to a compound eye, it has many eyelets arranged on a hemisphere. Each eyelet has its own lens and only a single sensing element - an LED. Unlike a compound eye, our eyelets face the center of the hemisphere and are optically isolated from each other. Most importantly, each eyelet can also emit light as a focused beam directed at the center of the hemisphere. The hemisphere provides accurate geometrical alignment, optical isolation between LEDs, and mechanical support and heat sinking for the LEDs. In the top figure, one LED illuminates the sample from a specific angle, while all other LEDs measure the reflected light at many other angles.

In the bottom figure, a different LED illuminates the sample from a new angle, and the remaining LEDs, including the previous illuminator, measure the reflected light. This process is repeated until all desired light patterns were activated.

3.1. Eyelets Placement on the Hemisphere

We used a geodesic tessellation to produce a relatively uniform and symmetric distribution of LEDs over a hemisphere. Starting from an octahedron incribed in a unit sphere centered at the origin, we consider just the four upper triangular faces and disregard the bottom four. Then we use the midpoints of the edges to subdivide each triangle in four new ones. We extend these midpoints outward from the origin until they also lie on the unit sphere. In this way, we can iteratively subdivide the hemisphere into finer and finer tessellations. This procedure produces 4^n, $n = 1, 2, 3, \ldots$ triangles on the hemisphere. The radius r of a sphere for LED diameter of d (enclosed within each triangle) is $r = \frac{\sqrt{3}d}{2\sin\frac{\pi}{2^{n+1}}}$. The lengths of the edges can vary by a factor as high as 1.73, but finer tessellations reduce the impact of this non-
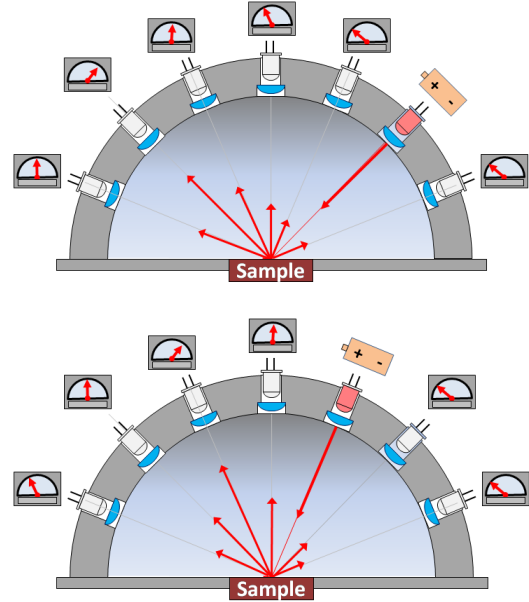

Figure 3. **Basic structure and operation. The device consists of an aluminum hemisphere with many embedded LEDs, all pointing toward the center of the hemisphere. A lens is used with each LED to improve the optical performance. During operation, each LED is turned on momentarily. While one LED emits light, all others measure the reflected light from the sample (top). Next, a different LED is chosen to emit light, and the remaining ones (including the previous emitter) measure the reflected light(bot).**

uniformity. If we had hexagonal lenses (or LEDs), a better tessellation with a nearly 100% fill factor would be possible using a hexagonal geodesic dome, much like arrangements of many compound eyes found in nature.

For BRDF measurement, we would like to very uniformly illuminate the sample surface. Different LEDs, however, produce very different illumination patterns, even for the same rated view angle. Fig 4(a) shows an example of this non-uniformity. To produce more even illumination, we added a lens to each eyelet. We placed the lens at its focal length distance from the approximate optical center of the LED creating telecentricity of the chief ray (only) [22] as seen in Fig 4(bottom). The result shown in Fig 4(b) has better light distribution and better approximation of a distant light source.

4. Radiometric Calibration

4.1. LED Dynamic Range

High-dynamic range photosensors are important for capturing the full range of BRDF measurements. To compare sensors with different characteristics, we represent dynamic range as $log_2 \frac{I_{max}}{I_{min}}$, where I_{max} is the maximum intensity (just before saturation) level that a sensor can measure, and I_{min} is the minimum (just noticeable) level above 0. This
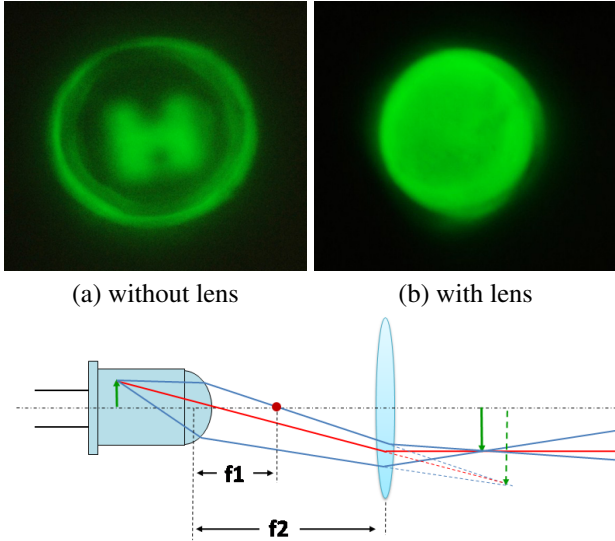
(a) without lens   (b) with lens

Figure 4. **An LED illumination pattern can be very non-uniform as shown in (a). Placing a lens at its focal length distance form the aperture of the LED (bottom) forms a beam with telecentric chief rays (only). This results in a better illumination distribution as shown in (c).**

definition, also known as the "range of f (or shutter) stops" is very intuitive for image sensors and applies to other sensors equally well.

To measure an LED's dynamic range, we place it in front of a strong light source (a halogen light with a condenser lens), attenuate the light using different neutral density filters, and measure the voltage output of the LED. The results are summarized in Table 1. In the table, λ is the peak emitting wavelength of the LED, and V_{max} is the maximum readout in millivolts. V_{min} is the minimum measurable readout (i.e. higher than the readout in darkness) after applying the greatest attenuation. Att. is the maximal attenuation used, and 'DR' is the dynamic range expressed in f-stops. The measured dynamic range of the LEDs ranges from 12 to 20 f-stops, which is very high. By contrast, the dynamic range of consumer cameras (such as the Nikon D70 and Canon EOS20D) is between 6 and 8 f-stops. For the yellow and red LEDs, our filter was not able to sufficiently reduce the signal level. We estimated the dynamic range based on the linear response of the LED (see below) in this range.

4.2. LED Response Functions

We must determine the LED response functions in order to convert their measured voltages to linear irradiance values. Fig 5 shows the setup used to measure the response of each of our LEDs. We place a white LED source and one of our other LEDs (blue, green, yellow or red) as the detector inside an integrating sphere. Using a regulated power supply, we drive different current levels through the white

LED	λ	V_{min}	V_{max}	Att.	DR
Blue	465	3	2300	1/4096	12
Green	525	5	1930	1/8192	13
Yellow	590	320	1740	1/8192	19*
Red	625	430	1650	1/8192	20*

Table 1. **Dynamic ranges of different LEDs.** λ is the peak emitting wavelength of the LED. V_{max} is the maximal readout in millivolts, and V_{min} is the readout after applying max. attenuation. Att. is the attenuation factor. DR is the dynamic range expressed in f-stops. (*) values are estimates.
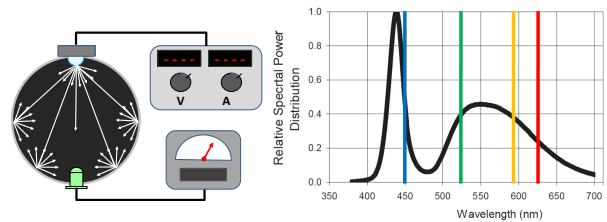

Figure 5. **Response function measurement setup. Left: we place a white LED source and one of our other LEDs (blue, green, yellow or red) as the detector inside an integrating sphere. The source LED radiance is directly proportional to the current through it. We compute the detector's response function by driving different currents through the source LED and measuring the voltage across the detector. Right: the white LED spectral distribution (shown in black) is wide enough to excite all of our LEDs. This allows us to compare the response functions of different LEDs relative to a common light source.**

LED. Keeping this current relatively low ensures that the LED operates in the linear region shown in Fig 1. Because the source LED radiance varies linearly with current, measuring the detector voltage for each source current gives us the detector's response function.

The measured response curves are shown in Fig 6. All the LEDs have highly non-linear responses, which explains their high dynamic range, but also suggests that the accuracy of their measurements decreases at higher irradiances. The blue and green LEDs (InGaP) are less sensitive, and their responses rises less sharply, than the red and yellow (AlGaInP) ones.

In addition to knowing each LED's response function, we must also know the relative responses between each pair of LEDs in our system. Generally speaking, LEDs are sensitive to wavelengths equal to or shorter than the wavelength of light they emit. A red LED will sense a blue LED, but not vice versa. Since LED spectra are not delta functions, LEDs with similar peak emission frequencies (such as our the red and yellow LEDs) can sense each other, but their responses are different. Using a similar methodology to that described above, we measured the response of each color LED to other colors capable of exciting it. These functions were similar to the functions shown above.
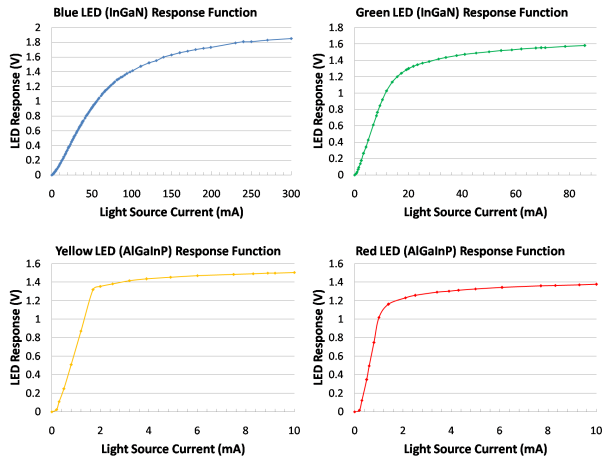
Figure 6. **LEDs response functions for a white light source. All the LEDs have highly nonlinear responses. Blue and green LEDs (InGaP) are less sensitive and have different response function than the red and yellow (AlGaInP)ones.**

4.3. Dark Current Noise

LEDs, like the photodetectors in CMOS and CCD image sensors, generate a small amount of current even in darkness. This current results from thermal energy, not incident light. The dark current is modeled by a temperature dependent Poisson distribution. To measure the mean (which is also the variance) of this dark current bias, we average many measurements in complete darkness. We can average because the response functions of the LEDs are nearly linear at low current levels. We convert the noise values to irradiance space using the inverse response function. We subtract these irradiance values from our later applied irradiances, including any subsequent calibrations that include a dark current component.

5. Geometric Calibration

If left uncorrected, the varying radiation patterns for each LED and geometrical inaccuracies of the device itself will lead to measurement errors. To calibrate to device, we measure the response of each LED to an isotropic light source at the material sample location.

Fig 7(a) shows our experimental setup for this process. We covered the bottom half of a small spherical diffuser with reflective material, then placed it at the center of the device. We sand the surface of a white LED to better diffuse the light it emits, put it at the bottom of the diffuser, and insert a baffle to prevent the LED from directly illuminating the top half of the diffuser. The spherical diffuser both integrates and diffuses the light, so the result is a nearly (1% variation) isotropic light source over the top hemisphere of the diffuser, as shown in Fig 7(b). All LEDs of a given color should measure the same intensity on the surface of the diffuser, but they do not because of geometric inaccuracies and
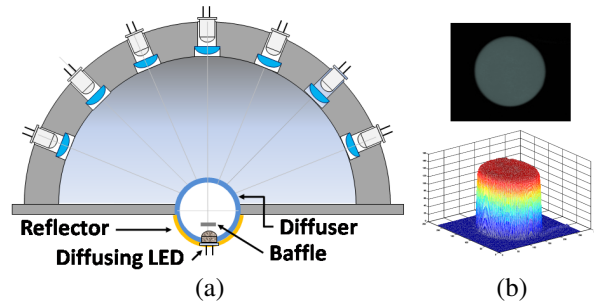

Figure 7. **Geometric calibration.** (a) **We create a small anisotropic light source using a spherical diffuser. A baffle prevents the LED at the bottom of the diffuser from directly illuminating the top half of the diffuser. We place the light source at the center of the device and measure the response from the LEDs. (b) This image and graph of the illuminated hemisphere show that the radiant light is nearly anisotropic. The intensity variation is roughly 1%.**

photoelectric variations. We measure and record the variations between LEDs for compensation later.

6. Stray Light and Internal Scattering

Finally, we must address one more issue: stray light and internal scattering. We first place a light trap at the material sample location and record the measured signal for each LED emitter-detector combination. This allows us to cancel stray light that exists in the measurement device. However, there can still be unwanted secondary and higher order reflections inside the hemisphere. Fig 8 describes how we minimize the unwanted effects caused by multiple reflections. Eyelets placement and telecentric optics significantly reduce detectors' sensitivity to non-radial rays. For radial rays, most of the light that enter the eyelets is either absorbed or passes though (into a dark room/box). Depending on the fill factor, some of the light will hit the hemisphere black wall. Due to the geometry of the device, most of the non-absorbed part (main lobe purple and green rays in the figure) will be retro-reflected back to the illuminating LED, which is not measuring any reflectance. This limits the unwanted stray light to the diffused part of third or higher order reflections.

7. Multi-Spectral BRDF

Because LEDs emit light at precise bandwidths and have a natural discriminative spectral response, we can use them for active or passive multi-spectral BRDF acquisition. One option is to use multi-band LEDs, which would allow us to emit and measure different colors from the same location. Multi-band LEDs, however, are currently limited to three bands and do not produce the same beam pattern for all bands, making them difficult to use. Instead, we dither different LEDs to increase the spectral resolution of our device. Fig 9 shows a schematic view of our LED arrange-
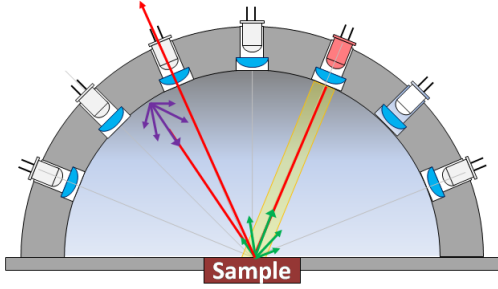
Figure 8. **Internal scattering. Telecentric optics ensures that eyelets are mostly sensitive to radial rays. Due to the hemisphere geometry, most of the unwanted high order radial reflections are retro-reflected to the LED that emits light, thus not interfering with the measurement.**
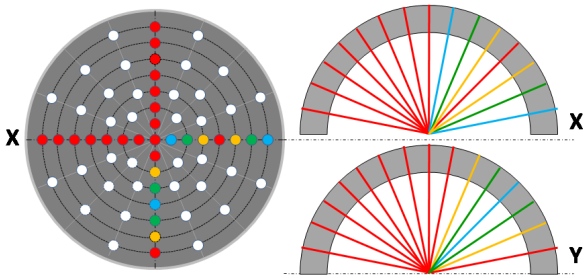

Figure 9. **LED arrangement for multi-spectral data acquisition. Different color LEDs are placed along the two main (most dense) axes. Red LEDs are put opposite to these LEDs to capture the mirror direction ray. Reciprocity provides the reverse direction. The rest of the LEDs (some of them are shown in white) provide additional, more sparse, information. These LEDs can be either red ones, which can sense all other LEDs, or white ones, which all other LEDs can detect.**

ment. Our hemisphere has two main axes where the LEDs are most dense. We spread the colored LEDs along one half of each axis. The LEDs on the remaining halves (shown in red) and the rest of the LEDs (shown in white) can either be red or white. Red LEDs can sense all the other ones, and all the LEDs can sense white ones. BRDF reciprocity provides the reverse direction for the same wavelength.

8. Multiplexed Illumination

Multiplexed illumination increases the measurement signal to noise ratio (SNR) [16]. Ghosh *et al.* also used multiplexed illumination to reduce the time needed for BRDF measurement[5]. In our case, multiplexing is a little more complex because each emitting LED cannot be used as a detector. Thus, we need to show multiplexing is still possible. Our basic equation system for recovering the BRDF is:

$$
\begin{bmatrix} m_1 \\ m_2 \\ \ldots \\ m_n \end{bmatrix} = \begin{bmatrix} b_{11}*r_{11} & b_{12}*r_{12} & \ldots & b_{1n}*r_{1n} \\ b_{21}*r_{21} & b_{22}*r_{22} & \ldots & b_{2n}*r_{2n} \\ & \ldots & & \\ b_{n1}*r_{n1} & b_{n2}*r_{n2} & \ldots & b_{nn}*r_{nn} \end{bmatrix} \begin{bmatrix} \cos\theta_1 L_1 \\ cos\theta_2 L_2 \\ \ldots \\ cos\theta_n L_n \end{bmatrix}
\tag{2}
$$

Here, m_i is the measured value at LED i, and $b_{ij} \in \{1, 0\}$ indicates the LEDs activated for each basis vector. $r_{ij} = \alpha_{ij} f_{r(ij)}$ is the BRDF coefficient $f_{r(ij)}$ that we wish to recover multiplied by the known calibration factor α_{ij} of the i, j LED pair. L_i is the intensity of LED i, and θ_i is the incident angle of LED i.

For n LEDs, there are $\frac{n^2-n}{2}$ unique BRDF coefficients to recover. $f_{r(ij)} = f_{r(ji)}$ due to BRDF reciprocity, and $f_{r(ii)}$ is not recoverable because the retro-reflective ray cannot be measured by the LED emitting the light. If b LEDs are on, only $(n - b)$ measurements are obtained and the number of different illumination patterns required is

$$
\frac{\frac{1}{2}(n^2 - n)}{n - b}
\tag{3}
$$

We know that the optimal multiplexed illumination basis is based on a Hadamard code of length $n + 1$, where $\frac{n+1}{4}$ is an integer[16]. This basis consists of n different illumination patterns for n LEDs. For each measurement, $\frac{n+1}{2}$ LEDs are on and $\frac{n-1}{2}$ are off. If we set $b = \frac{n+1}{2}$ in Equation 3, we see that the number of illumination patterns required for our setup using optimal illumination is exactly n. These are the patterns provided by the original Hadamard basis.

Since LED responses are non-linear and differ from band to band, multiplexed illumination can only be used when the emitted light is the same for all LEDs. Therefore, when different LEDs are used for multi-spectral BRDFs, they need to be multiplexed separately for each emitted bandwidth. There is no restriction when different LEDs are used as detectors.

9. Prototype Implementation

Our prototype, shown in Fig 10, consists of the measurement head (the hemisphere) and the controller. The hemisphere was machined from a single piece of aluminium using a CNC machine. This provides accuracy, mechanical strength and heat dispersion for the LEDs. The hemisphere was painted matte black to reduce unwanted inter-reflections. Our prototype contains 86 eyelets with a total of 7310 ($86*(86-1)$) possible illumination-reflection pairs. The controller contains a signal amplifier, an A/D converter, a micro-controller, and a communication unit in one board. A second extension board contains the LED control logic (multiple extension boards can be added to increase the number of LEDs). The controller receives a sequence of illumination patterns from a host computer via an RS232 connection, executes them one by one, and sends the measurements back the host for processing. The speed of our prototype is limited by the communication speed to the host. It can complete a (low density) BRDF measurement in roughly
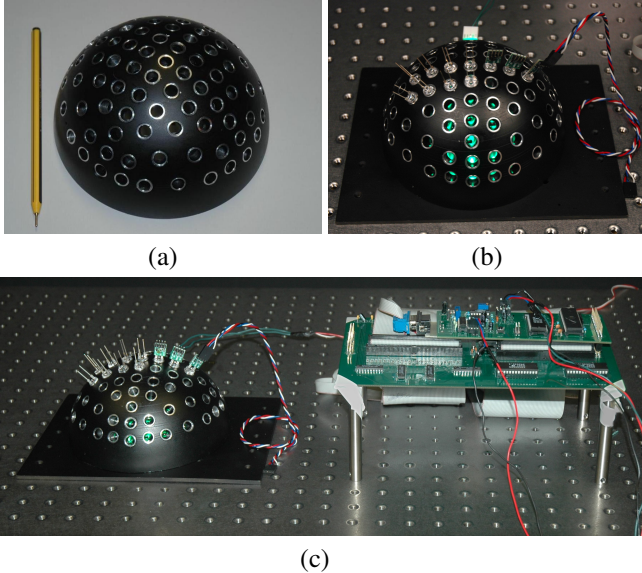
(a)

(b)

(c)

Figure 10. **Our prototype. (a) The measurement head, an aluminium hemisphere. (b) The measurement head with all lenses and a few LEDs installed. The green glow is the reflection from the table of one illuminating LED. The tiny boards mounted on the hemisphere are LED control circuits. (b) The complete system, including the measurement head and the main controller board. The board contains a signal amplifier, an analog to digital converter, a micro-controller, LED control logic, and a communication unit.**

6 seconds. See section 11 for a discussion about the theoretical speed limit our approach.

10. Processing and Results

We captured data of materials ranging from a very diffused yellow sponge to metallic specular silver paint. We then computed multi channel (RGB) images from the multispectral BRDFs data obtained by our prototype. We used push-pull method [6] to interpolate the captured data for rendering

The results are shown in Figures 11 and 12. Fig 11(a),(c) shows captured images of a red fabric and a metallic silver paper wrapped around a cylinder. Fig 11(b),(d) show rendering results using our computed BRDF and the camera's (Nikon D70) response function. We can see that the results are very similar (up to the fine texture information that was not captured by the BRDF measurement).

Fig12 shows a rendering of the Stanford Bunny model using different material BRDFs, from the very diffused yellow sponge to a highly specular silver paint.

11. Speed

Although parametric low order BRDF acquisition (with an optical low pass to prevent aliasing) takes only a few minutes using basis functions [5], high resolution BRDF capture is still very time-consuming. In this section, we esti-
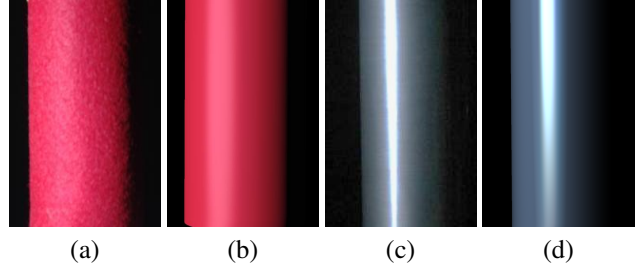

(a)   (b)   (c)   (d)

Figure 11. **(a),(c) Captured image of a cylinder wrapped with red fabric and metallic silver paper. (b),(d) Rendered image using captured BRDF of the red fabric and the metallic paper respectively. The image in (c) exhibits some saturation effect. The colors of both objects were rendered using our multi-spectral BRDF data.**
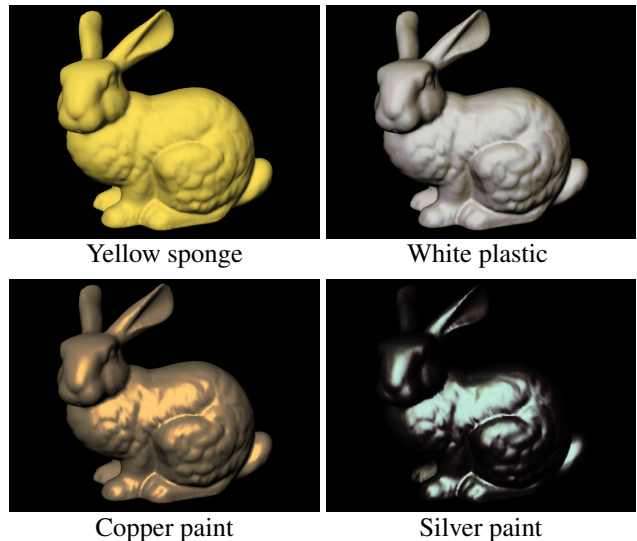

Yellow sponge   White plastic

Copper paint   Silver paint

Figure 12. **The Stanford Bunny rendered with our measured BRDF data. Diffused yellow sponge and white plastic (top), and metallic copper and silver paint (bottom).**

mate limits on the speed of our approach for high resolution BRDF measurement.

Special-purpose communication LEDs and circuits can switch on and off at rates up to 1GHz[17]. Our off-the-shelf, high luminosity LEDs and simple circuit are much slower than communication LEDs. To test the response time of our LEDs, we connected an LED source to a square wave generator, then measured the voltage across a detector LED using an oscilloscope. We used a simple, non-optimal circuit with a resistor load to discharge the LEDs at each cycle. Fig 13(a) shows the reference signal and the response time for the source-detector combination (hysteresis curve). We see that this circuit can operate at approximately 500Hz. The signal stabilizes in roughly $0.5ms$, then we have a $0.5ms$ window to read the signal before the reference signal drops. An additional $1ms$ is required to completely reset the LED before the next cycle can begin. During this $0.5ms$ read-out time, a high speed (16bit, 79dB SNR, 100M-Sample/sec) A/D converter (these are readily available today[1]), could read 50K
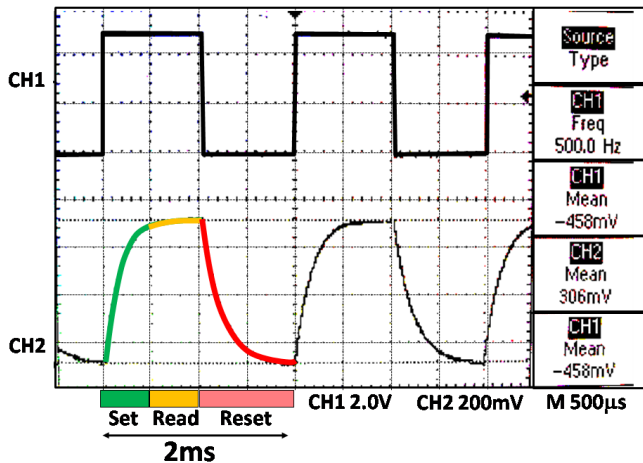
Figure 13. **LED response time for our simple circuit. Top: square wave signal sent to the transmitting LED at 500Hz. Bottom: Voltage at the receiving LED. Green - stabilization time, Yellow - time left for readout, Red - reset time.**

samples (LEDs). This corresponds to a density of 200×250 and nearly $50K^2$ combinations of illumination and reflection directions. Generating 50K light patterns at this rate (50K images, each having 250×200 pixels) would take 100 seconds. However, if we use only 1000 illumination directions with 50K reflection directions (which is still dense enough sampling) the time would drop to only 2 seconds. We believe that this time can be improved at least tenfold using better LED drive circuits and multiple A/D converters operating in parallel. Such high-speed BRDF acquisition would allow measurement of time-varying BRDFs[20] for very rapidly changing materials such as fast drying paint.

12. Conclusion

We presented a novel BRDF measurement device that uses only LEDs for illumination and measurement. We investigated the basic characteristics of high luminosity LEDs as light detectors, including their response functions, dynamic ranges and operating speeds. We presented a prototype device and example renderings using our acquired BRDF data. Our design is significantly simpler than existing designs and is, theoretically, capable of very high speed, high density BRDF acquisition (measured in seconds).

References

[1] Analog devices; http://www.analog.com/en/.

[2] K. Dana. BRDF/BTF measurement device. *International Conference on Computer Vision*, 2:460–6, 2001.

[3] P. Dietz, W. Yerazunis, and D. Leigh. Very Low-Cost Sensing and Communication Using Bidirectional LEDs. *Ubiquitous Computing, 5th International Conference, Seattle, WA, USA*, pages 175–191, 2003.

[4] J. Edmond, H. Kong, and C. Carter. Blue LEDs, UV photodiodes and high-temperature rectifiers in 6H-SiC. *Physica B*, 185(1-4):453–460, 1993.

[5] A. Ghosh, S. Achutha, W. Heidrich, and M. OToole. BRDF Acquisition with Basis Illumination. *IEEE International Conference on Computer Vision (ICCV)*, 2007.

[6] S. J. Gortler, R. Grzeszczuk, R. Szeliski, and M. F. Cohen. The lumigraph. In *SIGGRAPH '96: Proceedings of the 23rd annual conference on Computer graphics and interactive techniques*, pages 43–54, New York, NY, USA, 1996. ACM.

[7] J. Han and K. Perlin. Measuring bidirectional texture reflectance with a kaleidoscope. *Int. Conference on Computer Graphics and Interactive Techniques*, pages 741–748.

[8] T. Hawkins, P. Einarsson, and P. Debevec. A dual light stage. *Proceedings of the Eurographics Symposium on Rendering (Rendering Techniques)*, pages 91–98, 2005.

[9] S. Kuthirummal and S. K. Nayar. Multiview Radial Catadioptric Imaging for Scene Capture. *ACM Trans. on Graphics (also Proc. of ACM SIGGRAPH)*, Jul 2006.

[10] S. Marschner, S. Westin, E. Lafortune, and K. Torrance. Image-based bidirectional reflectance distribution function measurement. *App. Opt*, 39:2592–2600, 2000.

[11] W. Matusik, H. Pfister, M. Brand, and L. McMillan. Efficient isotropic BRDF measurement. *Proc. of the 14th Eurographics workshop on Rendering*, pages 241–247, 2003.

[12] F. Mims III. Sun photometer with light-emitting diodes as spectrally selective detectors. *Applied Optics*, 31(33):6965–6967, 1992.

[13] F. Nicodemus, N. B. of Standards, and U. States. *Geometrical Considerations and Nomenclature for Reflectance*. US Dept. of Commerce, National Bureau of Standards: for sale by the Supt. of Docs., US Govt. Print. Off., 1977.

[14] P. Peers, T. Hawkins, and P. Debevec. A reflective light stage. *USC Institute for Creative Technologies Technical Report ICT-TR-04.2006*, Dec 2006.

[15] H. J. Round. A Note on Carborundum. *Electrical World*, 49:309, 1907.

[16] Y. Schechner, S. Nayar, and P. Belhumeur. Multiplexing for Optimal Lighting. *Pattern Analysis and Machine Intelligence, IEEE Tran. on*, 29(8):1339–1354, 2007.

[17] E. Schubert. *Light-Emitting Diodes*. Cambridge University Press, 2006.

[18] W. Snyder, A. Inc, and M. Burlington. Definition and invariance properties of structured surface BRDF. *IEEE Tran. on Geoscience and Remote Sensing*, 40(5):1032–1037, 2002.

[19] K. Sumino, Y. Mukaigawa, and Y. Yagi. High Speed Measurement of BRDF Using an Ellipsoidal Mirror. *ACCV*, 2007.

[20] B. Sun, K. Sunkavalli, R. Ramamoorthi, P. Belhumeur, and S. Nayar. Time-Varying BRDFs. *IEEE Transactions on Visualization and Computer Graphics*, Mar 2007.

[21] G. Ward. Measuring and modeling anisotropic reflection. *ACM SIGGRAPH*, 26(2):265–272, 1992.

[22] M. Watanabe and S. Nayar. Telecentric Optics for Focus Analysis. *IEEE Transactions on Pattern Analysis and Machine Intelligence*, 19(12):1360–1365, Dec 1997.